DOI: 10.21276/sjet.2016.4.7.2

Scholars Journal of Engineering and Technology (SJET) **ISSN 2321-435X (Online)**
Sch. J. Eng. Tech., 2016; 4(7):301-307 **ISSN 2347-9523 (Print)**

(An International Publisher for Academic and Scientific Resources)
www.saspublisher.com

Research Article

Computation of Aerodynamic load on Protuberance over Satellite Launch Vehicle at Supersonic Speed

R. C. Mehta
Department of Aeronautical Engineering, Noorul Islam University, Kumaracoil, Thuckalay 629180, India

***Corresponding author**
R. C. Mehta
Email: drrakhab.mehta@gmail.com

Abstract: This paper presents numerical simulations to compute the aerodynamic load on protuberance for a typical launch vehicle. Surface pressure coefficients over the satellite launch vehicle are computed by solving axisymmetric time-dependent compressible Euler equations. The governing fluid flow equations are discretized in spatial coordinates employing a finite volume approach, which reduces the equations to semi-discretized ordinary differential equations. Temporal integration is performed using multi-stage Runge-Kutta time stepping scheme. A local time-step is used to achieve steady state solution. The novelty of the current numerical scheme is to block the grid corresponding to the protuberance. The entire flow field around the protuberance is analyzed with the help of Mach contour plots. The numerical scheme captures all the essential flow field features of high speed flow such as a shock wave in front of the protuberance and expansion fan on the shoulder and wake flow behind the protuberance. The numerical results are validated with experimental data in heat shield region of the launch vehicle for free stream Mach number 1.2, 1.6 and 2.0. The pressure distributions on the protuberance are required to maintain the structural integrity of the launch vehicle.
Keywords: Aerodynamic, CFD, Compressible flow, Satellite launch vehicle.

INTRODUCTION

The satellite launch vehicle has protuberance of varying geometrical shape and size to accommodate many components outside the core of the rocket. Computations of pressure coefficients as function of freestream Mach number during the ascent trajectory over the protuberance are essential in order determine the size and spacing of fasteners and underlying support structure. The presence of protuberance drastically alters flow field in the vicinity of the protuberance. Moreover, it also creates a local bow shock wave formation ahead of the protuberance.

McConnel [1] has experimentally investigated flowfield characteristics on an axisymmetric collar mounted protuberance on a cylindrical body. Experimental analyses of flowfield and unsteady pressure fluctuations ahead of two-dimensional forward facing step have been reported in Ref. [2] and [3]. Applebaum *et al.* [4] have presented numerical methodology to compute the protuberance aerodynamic loads for the NASA Ares I rocket program employing unstructured USM3D flow solver. Oamar *et al.* [5] have presented aerodynamic characteristic of an axisymmtric surface protuberance attached to a spherical nosed body of revolution for Mach number ranging from 3 to 8. Most of the research work focused on experimental approach for forward ramp, square or rectangular cross-section protuberance. Few papers have been found on the numerical simulations of axisymmetric surface protuberance.

In the present paper, computational fluid dynamic simulations are carried out to compute pressure coefficients on the protuberance. A numerical simulation of time-dependent compressible axisymmetric Euler equations is carried out employing multi-stage Runge-Kutta time-stepping scheme. The numerical scheme is second accurate in space and time. A local time stepping is used to achieve steady state solution. The purpose of the present study is to obtain the pressure coefficients for freestream Mach number 1.2, 1.6 and 2.0. Comparison between numerically computed pressures distributions over a satellite launch vehicle with wind tunnel data are made that will provide reliability and confidence in employing CFD simulations. The numerical solutions are obtained employing the structured grid arrangement with indigenous developed Euler flow solver. The structural engineer will use this data to compute buckling and bolt placement/strength on the core structure due to the presence of the protuberance. The external pressure distribution is useful for venting analysis to estimate pressure differential across the skin. The novelty of the present method is to block the grid correspond to the size of the protuberance. Thus the numerical analysis is flexible to study different size of

protuberance to satisfy the structural integrity of the launch vehicle. It is worth noting that if a protuberance fails because of the data in the vehicle aerodynamic/structure data book, further analysis can easily carried out employing the present blocking grid arrangement method. The computations of surface pressure will be helpful for adequate for preliminary design of the protuberance support system.

GOVERNING EQUATIONS

The governing fluid dynamics equations are time-dependent compressible axisymmetric Euler equations are written as

$$\frac{\partial \mathbf{U}}{\partial t}+\frac{\partial \mathbf{F}}{\partial x}+\frac{1}{r}\frac{\partial (r\mathbf{G})}{\partial r}+\frac{\mathbf{H}}{r}=0 \tag{1}$$

where

$$\mathbf{U}=\begin{bmatrix}\rho\\ \rho u\\ \rho v\\ \rho e\end{bmatrix},\quad \mathbf{F}=\begin{bmatrix}\rho u\\ \rho u^2+p\\ \rho uv\\ (\rho e+p)u\end{bmatrix},\quad \mathbf{G}=\begin{bmatrix}\rho u\\ \rho uv\\ \rho v^2+p\\ (\rho e+p)v\end{bmatrix},\quad \mathbf{H}=\begin{bmatrix}0\\ 0\\ p\\ 0\end{bmatrix}$$

are the **U** state vector conserved quantities with ρ, u, and v denoting the density, velocity components in x and r-direction respectively, and e specific total internal energy, respectively, and inviscid flux vectors, $\boldsymbol{F}$, and $\boldsymbol{G}$ and $\boldsymbol{H}$ is source vector. With the ideal gas assumption, the pressure and total enthalpy can be expressed as

$$\rho\, e=\frac{p}{(\gamma-1)}+\frac{1}{2}\rho\left(u^2+v^2\right) \tag{2}$$

where γ is the ratio of specific heats. The following section describes a finite volume scheme in conjunction with multistage Runge-Kutta time stepping scheme to solving the axisymmetric compressible Euler equations.

Finite Volume Scheme

To facilitate the finite volume spatial discretiztion in the computation method, Equation (1) can be written in the integral form over a finite volume fixed in time as

$$\frac{\partial}{\partial t}\int_{\Omega}\mathbf{U}\,d\Omega+\int_{S}\bar{r}\left(\boldsymbol{F}dr-\boldsymbol{G}dx\right)+\int_{\Omega}\boldsymbol{H}d\Omega=0 \tag{3}$$

where Ω is the arbitrary control volume with the closed boundary $\partial\Omega$ and control surface S, and outward normal facing unit vector n. The domain is divided into a finite number of hexahedral cells, and Eq. (1) is applied to each cell. The state variables **U** are volume-averaged values. The discretization of Eq. (1) follows discretization in space and time is done separately. A finite volume cell is specified by eight corners, which are connected by straight lines. The discrete values of the flow quantities are calculated at the centre of the cell. Simple vector information can be used to obtain side and surface vectors relationship along with the computational cell volume. A system of ordinary differential equations can be obtained by applying Eq. (3) to cells formed by six surfaces as

$$r_c A_{i,j}\frac{d\left(U_{i,j}\right)}{dt}+Q\left(U_{i,j}\right)-D\left(U_{i,j}\right)=0 \tag{4}$$

where $\Omega_{i,j}$ is the volume of the cell, $Q_{i,j}$ is the convective fluxes out of the cell. The summation of the flux vectors over the six faces of the hexahedral cell is done using the average flux on each cell face. The above scheme reduces the centre differences scheme. It will allow odd and even nodes coupling.

Artificial Dissipation

In order to prevent odd-even point decoupling and oscillations in vicinity of shock waves, and to obtain rapid convergence to the steady state, artificial dissipative terms $D_{i,j,}$ are added to Eq. (4). The artificial dissipation model considered in the present paper is based on the work of Jameson, Schmidt, and Turkel [6]. A blend of forth and second differences is used to provide third-order back-ground dissipation at shock waves, and is given by

$$D_{i,j}=\left(D_x+D_r\right)U_{i,j}$$

Where

$$D_x=d_{i+\frac{1}{2},j}-d_{i-\frac{1}{2},j}$$

$$D_r=d_{i,j+\frac{1}{2}}-d_{i,j-\frac{1}{2}}$$

The dissipative fluxes $d_{i+½,j,k}$ are defined as blend in of first and third differences

$$d_{i+\frac{1}{2},j} = \frac{(\Delta A)_{i+\frac{1}{2},j}}{\Delta t}\left\{\varepsilon^{(2)}_{i+\frac{1}{2},j}\left(U_{i+1,j} - U_{i,j}\right) - \varepsilon^{(4)}_{i+\frac{1}{2},j}\left(U_{i+2,j} - 3U_{i+1,j} + 3U_{i,j} - U_{i-1,j}\right)\right\} \quad (5)$$

The adaptive coefficients, $\varepsilon^{(2)}$ and $\varepsilon^{(4)}$ are

$$\varepsilon^{(2)}_{i+\frac{1}{2},j} = \kappa^{(2)}\, max\left(\nu_{i+1,j}, \nu_{i,j}\right)$$

$$\varepsilon^{(4)}_{i+\frac{1}{2},j} = max\left\{0, \left(\kappa^{(4)} - \varepsilon^{(2)}_{i+\frac{1}{2},j}\right)\right\}$$

Here ν is a shock sensing function based on pressure and can be written as

$$\nu_{i,j} = \frac{\left|\nu_{i+1,j} - \nu_{i,j} + \nu_{i-1,j}\right|}{\left|\nu_{i+1,j} - \nu_{i,j} + \nu_{i-1,j}\right|} \quad (6)$$

In the present computation the values of $\kappa^{(2)}$ and $\kappa^{(4)}$ are constants, taken equal to 1/4 and 1/256, respectively. The dissipative operators in the *r* are defined in a similar manner. The blend of second and fourth differences provided third-order background dissipation in smooth regions of the flow and first-order dissipation in shock waves.

Time-stepping scheme

The above spatial disretization reduces the governing equations to semi-discrete ordinary differential equations, temporal integration is carried out using multi-stage Runge-Kutta time-stepping scheme [6]. Suppressing the subscripts (*i*,*j*), the following steps are employed for the numerical integration

$$\begin{aligned} U^{(0)} &= U^n \\ U^{(1)} &= U^n - 0.6\frac{\Delta t}{\Delta\Omega}\left(\boldsymbol{R}^{(0)} - \boldsymbol{D}^{(0)}\right) \\ U^{(2)} &= U^n - 0.6\frac{\Delta t}{\Delta\Omega}\left(\boldsymbol{R}^{(1)} - \boldsymbol{D}^{(0)}\right) \\ U^{(3)} &= U^n - \frac{\Delta t}{\Delta\Omega}\left(\boldsymbol{R}^{(2)} - \boldsymbol{D}^{(0)}\right) \\ U^{n+1} &= U^{(3)} \end{aligned} \quad (7)$$

where *n* is the current time level, and *n*+1 is the new time level. ***R*** is the sum of the inviscid fluxes. In order to minimize the computation time, the evaluation of the dissipation term ***D*** is carried out only at the first stage, and then frozen for the subsequent stages. The numerical scheme is stable for a Courant number ≤ 2. A local time step is used to get steady state solution. The numerical scheme is second accurate in space and time.

Initial and Boundary Conditions

Initially the body is assumed to be immersed completely in the uniform freestream conditions. Four types of boundary conditions are required for the computation of flow field, i.e., wall, inflow, and outflow symmetric conditions. They are prescribed as follows: at the solid wall slip boundary condition is imposed. The flow properties in the image cell are taken as those of the adjacent boundary cell, except that the normal component of the velocity is reflected to ensure the impermeability condition. At inlet boundaries, all of the properties are imposed since the inflow is supersonic. At the out flow boundary, the two tangential velocity components are extrapolated from the interior, while at the inflow boundary they are specified as having far field values. The out flow is extrapolated from the values at the interior cells. The flow is tangent to the wall. The flow gradients of the other primitive variables are zero on the symmetry boundary ahead of the heat shield.

GRID GENERATION

In order to initiate numerical simulation of flow over the satellite launch vehicle, the physical space is discretized into non-uniform structured grid points. These body-oriented grids are generated using a finite element method [7] in conjunction with homotopy scheme [8]. The capsule computational region is divided by a number of grid points. Using these surface grid points as reference nodes, the normal coordinates is then described by stretched structured field points extending on ward up to the outer computational boundary. These stretched grids are generated in an orderly manner. Grid independent tests are carried out taking into consideration the effect of the computational domain, the stretching factor to control the grid intensity near the wall, the number of grid points in the axial and normal directions. The outer boundary of the computational domain is varied from 5 to 12 times the maximum diameter, *D*. To validate the code, the numerical results are compared with surface pressure distribution along the vehicle with the wind tunnel data [9] and they are found good agreement. This arrangement of grid is found to give a relative difference of about ±3% in the pressure peak value in the shoulder region of heat shield of the satellite launch vehicle with the

convergence criterion of $\left|\rho^{n+1} - \rho^{n}\right| \leq 10^{-5}$ between two successive iterations. After extensive grid independent test, 90×42 grid points are taken in the longitudinal and normal directions. Figure 1 shows the zoom view of the structured grid arrangement over the satellite launch vehicle. The protuberance is located downstream of the core where the flow once again attain freestream conditions. The computation is carried out by imposing no flux condition on the protuberance boundary. This approach is simple to accommodate the protuberance of complex geometrical shape over the core and can easily be accommodate in the flow solver. We have considered an axisymmtric protuberance attached to the core vehicle.

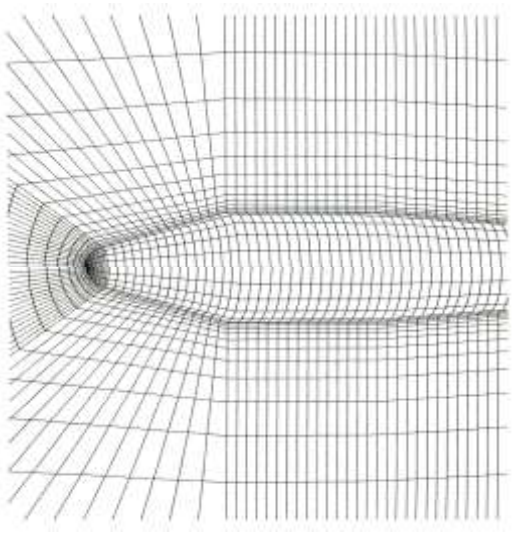

Fig-1: Zoom view of computational grid

RESULTS AND DISCUSSION

The numerical analysis is performed over the satellite launch vehicle to validate the above flow solver and also determine the recovery of the freestream once again over the vehicle. This will provide the location of the protuberance from the stagnation point of the heat shield

Flow characteristics over the satellite launch vehicle

The flow simulation over the complete vehicle will help to decide the location of the protuberance. The numerical computation is carried out for freestream Mach number 1.2, 1.6 and 2.0 and depicted in Fig. 2. A bow shock wave stands in front of the payload shroud and forms a region of subsonic flow around the stagnation region. An expansion fan over the shroud of the heat shield can also be observed in the Mach contour plots. It is interesting to observe from the Mach contour plots that the influence of flowfield domain coming close to the vehicle as the freestream Mach number increasing. The pressure coefficient at is computed using following expression

$$Cp = \frac{\left(\frac{p}{p_\infty} - 1\right)}{\frac{1}{2}\gamma M_\infty^{\,2}} \tag{8}$$

where M_∞ is freestream Mach number. The variations of surface pressure are shown in Fig. 3 for freestream Mach number 1.2, 1.6 and 2.0. The comparison between computed results with experimental data [7] shows some disagreement on the cylindrical region of the heat shield. This is attributed to pressure loss along the expansion fan, poor recovery of the pressure and separated flow on the boat tail region of the heat shield. The comparison between the experimental and numerical results are reasonably in agreement except in the boattail region. This disagreement may be due to the separation of flow in the boat tail region. The trend of the local normal load distribution is matching well with the experimental data.

Fig-2: Mach contours over the heat shield

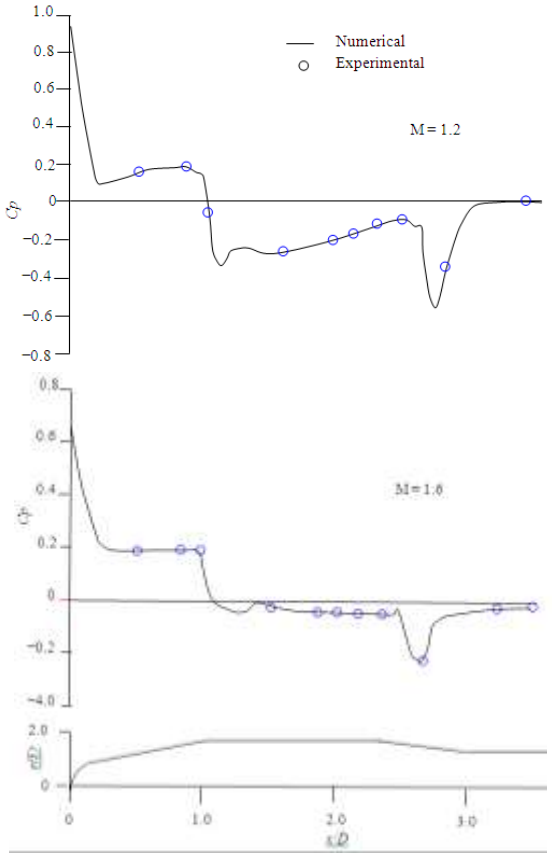

Fig-3: Variations of surface pressure coefficient along the satellite launch vehicle

Flowfield Analysis over the protuberance

The flowfield simulation over the satellite launch vehicle shows that freestream is achieved about downstream about 8 to 9 times the diameter *D* of the payload shroud. In order to save the computer time, the flow simulation is carried out in the region where the protuberance is situated. The protuberance is mounted rocket having diameter of 1.5m. The height of the protuberance is 0.28m and length is about 1.3m. The flowfield inside the protuberance are not computed by considering the boundary of the protuberance. Figure 4 shows the Mach contour plots in presence of the protuberance for freestream Mach number of 1.2, 1.6 and 2.0. It can be observed from the Mach contour plots that a formation of bow shock ahead of the protuberance and downstream of the protuberance a formation of wake region. The bow shock is found steeper with the increase of the freestream Mach number.

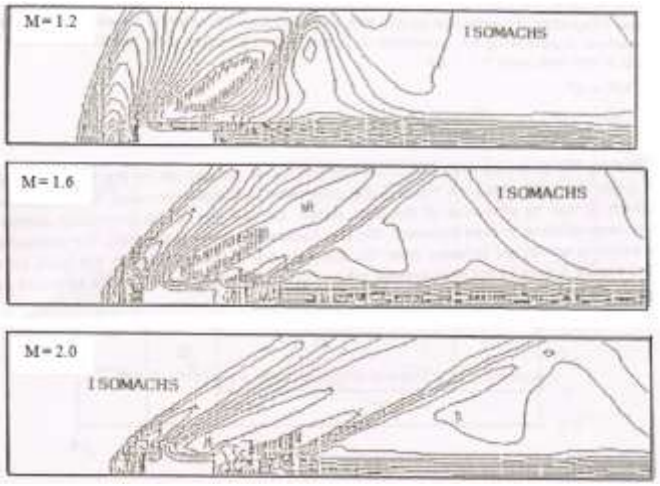

Fig-4: Mach contours over the protuberance

The surface pressure distribution over the front, along and back of the protuberance is depicted in Fig. 5. The front and back surfaces are indicated in the figure. In front of the protuberance a sudden increase of the surface is attributed to the presence of the bow shock as visualized in the Mach contour plots. The maximum pressure coefficient is found over the shoulder of the protuberance. It is interesting to note that the maximum surface pressure is decreasing with the increasing of the freestream Mach number. On the top surface of the protuberance, the remains near to constant value. Behind the protuberance, the pressure coefficient suddenly falls. Thus low pressure region is due to the formation of wake region in the downstream of the protuberance. The variations of surface pressure distribution show that the protuberance experiences compression and expansion on the front and the back side of the protuberance. Therefore, the pressure distributions are essential to maintain the structural integrity of the vehicle.

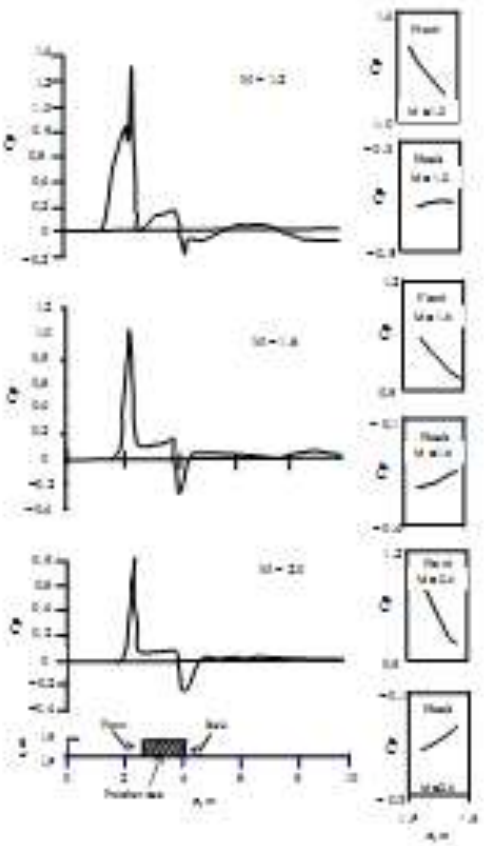

Fig-5: Variations of surface pressure coefficient along, front and back side of the protuberance

CONCLUSIONS

A numerical simulation of axisymmetric flow over a satellite launch vehicle and protuberance is carried out using multi-stage Runge-Kutta time stepping scheme in conjunction with finite volume method. A local time step is used to achieve steady-state solution. The novelty of the current numerical scheme is to block the flow computation inside the protuberance. This approach can be applied to accommodate different size and kind of the protuberance. The entire flow field around the satellite launch vehicle and the protuberance is analyzed with the help of Mach contour plots. The numerical scheme captures all the essential flow field features of high speed flow such as a shock wave in front of the rocket and the protuberance. The numerical results of the satellite launch vehicle are validated with experimental data in heat shield region for freestream Mach number 1.2, 1.6 and 2.0. The pressure distributions on the front, the top and the back sides of the protuberance is input quantity for the structural design of brackets/bolts in order to maintain the structural integrity of the vehicle.

REFERENCES

1. McConnel DG; Free flight observation of separated turbulent flow including heat transfer up to Mach 8.5, NASA TN-D 278, 1960.
2. Coe CE, Chyu WJ, Dvds Jr, JR; Pressure fluctuations underlaying attached and separated supersonic turbulent boundary layers and shock waves, AIAA paper, 73-998, 1973.
3. Kistler AL; Fluctuating wall pressure under a separated flow, Journal of Acoustic Society of America, 1964; 36(3): 543-550.
4. Applebaum M, Eppard M, Hall L, Blevins J; Protuberance aerodynamic loads for space launch vehicle systems using CFD, 29th AIAA Applied Aerodynamics Conference, Hawaii, AIAA 2011-3649, 2011.
5. Qamar A, Sanghi S; Aerodynamics characteristic of axisymmetric surface protuberance in supersonic regime, Engineering Applications of Computational Fluid Mechanics, 2012; 6(3):316-335.
6. Jameson A, Schmidt W, Turkel E; Numerical solution of Euler equations by finite volume methods using Runge-Kutta time stepping schemes, AIAA 81-1259, 1981.
7. Mehta RC; A quasi three dimensional automatic grid generation method, in the proceedings of the 25th National and International Conference on Fluid Dynamics and Fluid Power, IIT, Delhi, India, 1998; 89-98.
8. Shang JS; Numerical simulation of wing-fuselage interference, AIAA paper 81-0048, 1981.
9. Mehta RC, Sastry MS; Computational aerodynamic loads and coefficient for satellite launch vehicle, Indian Journal of Engineering and Material Sciences, 1997; 4(1): 41-48.